chemosensors

MDPI

Article

Bi_2S_3/rGO Composite Based Electrochemical Sensor for Ascorbic Acid Detection

Chengling Qu [1], He Li [1], Shuang Zhou [1], Guodong Li [2], Cheng Wang [1], Rony Snyders [3], Carla Bittencourt [3] and Wenjiang Li [1,*]

[1] Institute for New Energy Materials & Low-Carbon Technologies, School of Materials Science and Engineering, Tianjin University of Technology, Tianjin 300384, China; qcl_0710@163.com (C.Q.); lhtjut@126.com (H.L.); Zhous_prc@163.com (S.Z.); cwang@tjut.edu.cn (C.W.)

[2] State Key Laboratory of Inorganic Synthesis and Preparative Chemistry, College of Chemistry, Jilin University, Changchun 130012, China; lgd@jlu.edu.cn

[3] Plasma-Surface Interaction Chemistry (ChIPS), Research Institute for Materials Science and Engineering, University of Mons, 20 Place du Parc, 7000 Mons, Belgium; Rony.SNYDERS@umons.ac.be (R.S.); Carla.BITTENCOURT@umons.ac.be (C.B.)

* Correspondence: liwj@tjut.edu.cn; Tel.: +86-22-60214028

Abstract: The engineering of an efficient electrochemical sensor based on a bismuth sulfide/reduced graphene oxide (Bi_2S_3/rGO) composite to detect ascorbic acid (AA) is reported. The Bi_2S_3 nanorods/rGO composite was synthesized using a facile hydrothermal method. By varying the amount of graphene oxide (GO) added to the synthesis, the morphology and size of Bi_2S_3 nanorods anchored on the surface of rGO can be tuned. Compared to a bare glassy carbon electrode (GCE), the GCE modified with Bi_2S_3/rGO composite presented enhanced electrochemical performance, which was attributed to the optimal electron transport between the rGO support and the loaded Bi_2S_3 as well as to an increase in the number of active catalytic sites. Cyclic voltammetry (CV) and electrochemical impedance spectroscopy (EIS) analysis of Bi_2S_3/rGO/GCE demonstrate that the active Bi_2S_3/rGO layer on GCE plays an important role in the electrochemical behavior of the sensor. In particular, the Bi_2S_3/rGO/GCE sensor shows a wide detecting range (5.0–1200 μM), low detection limit (2.9 μM), good sensitivity (268.8 μA mM^{-1} cm^{-2}), and sufficient recovery values (97.1–101.6%) for the detection of ascorbic acid.

Keywords: Bi_2S_3; reduced graphene oxide; ascorbic acid; electrochemical sensor

check for updates

Citation: Qu, C.; Li, H.; Zhou, S.; Li, G.; Wang, C.; Snyders, R.; Bittencourt, C.; Li, W. Bi_2S_3/rGO Composite Based Electrochemical Sensor for Ascorbic Acid Detection. *Chemosensors* **2021**, *9*, 190. https://doi.org/10.3390/chemosensors9080190

Academic Editor: Dario Compagnone

Received: 2 June 2021
Accepted: 18 July 2021
Published: 23 July 2021

1. Introduction

Ascorbic acid (AA), as an essential biological molecule in the human blood, is indispensable for various physiological and metabolic activities. Therefore, it is important to develop facile and sensitive techniques to accurately determine amounts of AA for application in the pharmaceutical, chemical, cosmetic, and food sectors. Compared with traditional analysis methods, such as fluorimetry [1], colorimetry [2], voltammetry [3,4], flow injection analyses [5], spectrophotometry [6], and liquid chromatography [7], the electrochemical detection of AA is considered to be a simple low-cost method owing to its easy operation, high sensitivity and low detection limit [8,9]. However, the direct oxidation of AA on bare electrodes results in electrode surface fouling, high overvoltage, low sensitivity, poor reproducibility, and high interference with other biomolecules [10]. Therefore, it is important to choose an appropriate active material to modify glassy carbon electrodes (GCE) improving their selectivity and sensitivity towards an accurate AA determination.

Following the development of nanomaterials in electrochemical sensors, various materials such as organic redox mediators [11], nanoparticles [12], polymers [13], carbon nanotubes [14], and graphene [15] have been used as redox-active sites to modify the standard electrode surface, reducing the activation energy barrier of the electrochemical reaction and speeding up the electron transfer process [16]. Recently, bismuth sulfide

(Bi_2S_3) has attracted much attention as the electrochemically active material in gas sensors, photoresponsive devices, and solar cells due to its unique electronic and optical properties [17–21]. However, the poor intrinsic conductivity and easy agglomeration of Bi_2S_3 nanoparticles result in low sensitivity and narrow linear range in electrochemical detection limiting its practical applications [22]. Up to now, various strategies have been proposed to improve the electrochemical properties of Bi_2S_3. Graphene (GO) has been reported to be an ideal substrate material for the development of optimal nanocomposite sensing materials due to its surface properties and electronic transport properties [23,24]. Luo et al. reported on Cu/graphene nanocomposites as active layer for non-enzymatic glucose sensors, with good stability and selectivity [25]. Guo et al. [26] used MoS_2-rGO/ITO composites as active materials in electrochemical sensors to simultaneously detect uric acid (UA) and dopamine (DA). Yan et al. [27] synthesized rGO/Bi_2S_3 nanocomposites using thioacetamide as the sulfur source, and used these nanocomposites as the active layers with remarkable increases in the selectivity and sensitivity of the DA sensor.

In this work we describe a facile-yet-efficient strategy to engineer the structure of Bi_2S_3 nanostructures. The correlation among graphene content, Bi_2S_3 structure and electrochemical characteristics is evaluated. In addition, the Bi_2S_3/rGO modified glassy carbon electrode (GCE) is validated as active layer in electrochemical sensors for ascorbic acid (AA) detection. The fabricated Bi_2S_3/rGO/GCE as AA sensor presented a wide linear detection range, high sensitivity and good selectivity in the presence of various interfering compounds in aqueous phosphate buffer solutions. This work provided an additional step for improving the electrocatalytic activity of transition metal chalcogenides and expanding their applications in the field of electrochemical sensing.

2. Materials and Methods

2.1. Reagents

GO was prepared using graphite powder by the modified Hummers method [28]. Thiourea, thioacetamide (TAA), $Na_2S_2O_3$, $Na_2S{\cdot}9H_2O$, and bismuth nitrate [Bi $(NO_3)_3{\cdot}5H_2O$] were obtained from Shanghai Chemical Reagent Company (Shanghai, China). Disodium hydrogen phosphate (Na_2HPO_4), sodium dihydrogen phosphate (NaH_2PO_4), ascorbic acid (AA), and interferents were provided by Aladdin Reagent Co., Ltd. (Shanghai, China). The phosphate buffer (PBS, 0.1 M) was prepared by mixing $Na_2HPO_4{\cdot}2H_2O$ and $Na_2HPO_4{\cdot}2H_2O$. The pH of PBS was adjusted with HCl or NaOH. All chemicals were of analytical grade. Deionized water was used throughout the experiments.

2.2. Instruments

The morphology and crystal structure of the samples were determined by Environmental scanning electron microscope with a field emission gun (ESEM, Quanta FEG 250, Hillsboro, OR, USA) and transmission electron microscopy (TEM, Talos F 200 X, Waltham, MA, USA). The crystal phase structure and composition of Bi_2S_3 in the composite were analyzed by X-ray diffractometer (XRD, D/Max2500pc, Akishima-shi, Tokyo, Japan), Raman spectroscopy (Horiba Evolution, Minami-ku, Kyoto, Japan), and X-ray photoelectron spectra (XPS, ESCALAB250Xi, Waltham, MA, USA). The molecular structure and chemical composition of graphene materials were determined by Fourier transform infrared spectrometer (FT-IR, Perkin Elmer, Waltham, MA, USA). Electrochemical studies were measured by CHI 660E electrochemical analyser (Shanghai Chenhua Instrument Co., Ltd., Shanghai, China) using a conventional three-electrode system.

2.3. Synthesis of Bi_2S_3/rGO Nanocomposites

Bi_2S_3 samples were synthesized with different sulfur sources to determine the the sulfur source leading to nanostructures with best sensor activity. As shown in Figure S1 Bi_2S_3 the sample prepared with thiourea has a higher current response. This may be attributed to the higher specific surface area and presence of more active sites on Bi_2S_3 nanostructures prepared with thiourea which can improve the electrochemical performance

of the working electrode by accelerating electron transfer, compared with nanostructures synthesized with other sulfur sources.

Synthesis procedure: the GO was sonicated for 2 h in deionized water to form a solution of 1 mg mL^{-1}. Then, different amounts of Bi $(NO_3)_3 \cdot 5H_2O$ were added to the GO solution and stirred for 30 min (solution A). Based on the weight ratio of Bi $(NO_3)_3 \cdot 5H_2O$:GO, the nanocomposites were named Bi_2S_3/rGO-1 (4:1), Bi_2S_3/rGO-2 (2:1), Bi_2S_3/rGO-3 (1:1) and Bi_2S_3/rGO-4 (1:2), respectively. The thiourea was dissolved in 10 mL deionized water (solution B), Bi $(NO_3)_3 \cdot 5H_2O$ and thiourea in a molar ratio of 1:10. Next, solution B was slowly added into solution A with continuous stirring for 20 min. The resulting mixture was transferred into 100 mL Teflon lined stainless steel autoclave, sealed, and heated at 180 °C for 12 h in an electric oven, and the brownish-black products were centrifuged (at 7000 rpm for 5 min) and washed five times with deionized water and alcohol. Finally, the obtained Bi_2S_3/rGO products were dried for 5 h in a vacuum oven at 60 °C.

2.4. Sensor Fabrication

Firstly, the glassy carbon electrodes (GCEs) were carefully polished using Al_2O_3 powders (0.5 mm, and 0.05 μm) on a polishing cloth, successively washed with ethanol and deionized water and dried at room temperature. Next, 10 mg of Bi_2S_3/rGO sample was dispersed in the mixture solution containing 5.0 mL of N, N-Dimethylformamide (DMF) and 100 μL of Nafion for ultrasonic treatment for 20 min, obtaining homogeneous Bi_2S_3/rGO composite suspension. Then, 5.0 μL of the above Bi_2S_3/rGO suspension was coated on surface of the cleaned GCE, after drying in hot air for 10 min, the sensor fabricated with Bi_2S_3/rGO/GCE was obtained. Likewise, for comparison, the similar sensor based on rGO/GCE and Bi_2S_3/GCE were prepared.

3. Results

3.1. Characterization of Bi_2S_3/rGO

The morphology of the Bi_2S_3/rGO samples was characterized by SEM and TEM as shown in Figure 1. From SEM images (Figure 1a–d), it is clearly seen that well dispersed rod-like structures of Bi_2S_3 are formed on the surface of rGO in all Bi_2S_3/rGO samples. Moreover, we observed that when the weight ratio of Bi $(NO_3)_3 \cdot 5H_2O$: GO decreased from 4:1 to 1:2, the average size of Bi_2S_3 nanorods on the rGO sheets increased by three to five times. In contrast, pure Bi_2S_3 samples prepared using different sulfur sources in the absence of GO (Figure S2), are highly aggregated, indicating that GO plays an important role in dispersing nanoparticles during the hydrothermal synthesis. The interaction of Bi^+ with oxygen-containing groups of GO was reported to be responsible for the dispersibility of Bi_2S_3 nanorods [29]. It is worth noting that using an appropriate amount of GO in the solution resulted in higher interfacial contact between rGO sheets and Bi_2S_3 nanorods. As shown in Figure 1c, the Bi_2S_3 rods are wrapped around the thin rGO sheets in Bi_2S_3/rGO-3, this sample also presented the best electrochemical performance. From TEM images of Bi_2S_3/rGO-3 shown in Figure 1e,f, the diameter of Bi_2S_3 rods is about 50–120 nm and the length ranges from 0.4–2.3 μm. The Bi_2S_3 rods are mostly randomly distributed on the surface of rGO. In addition, the elemental mapping (Figure S3) further illustrates the good dispersion in the composite material, and the EDAX analysis indicates that the synthesized composite has high purity.

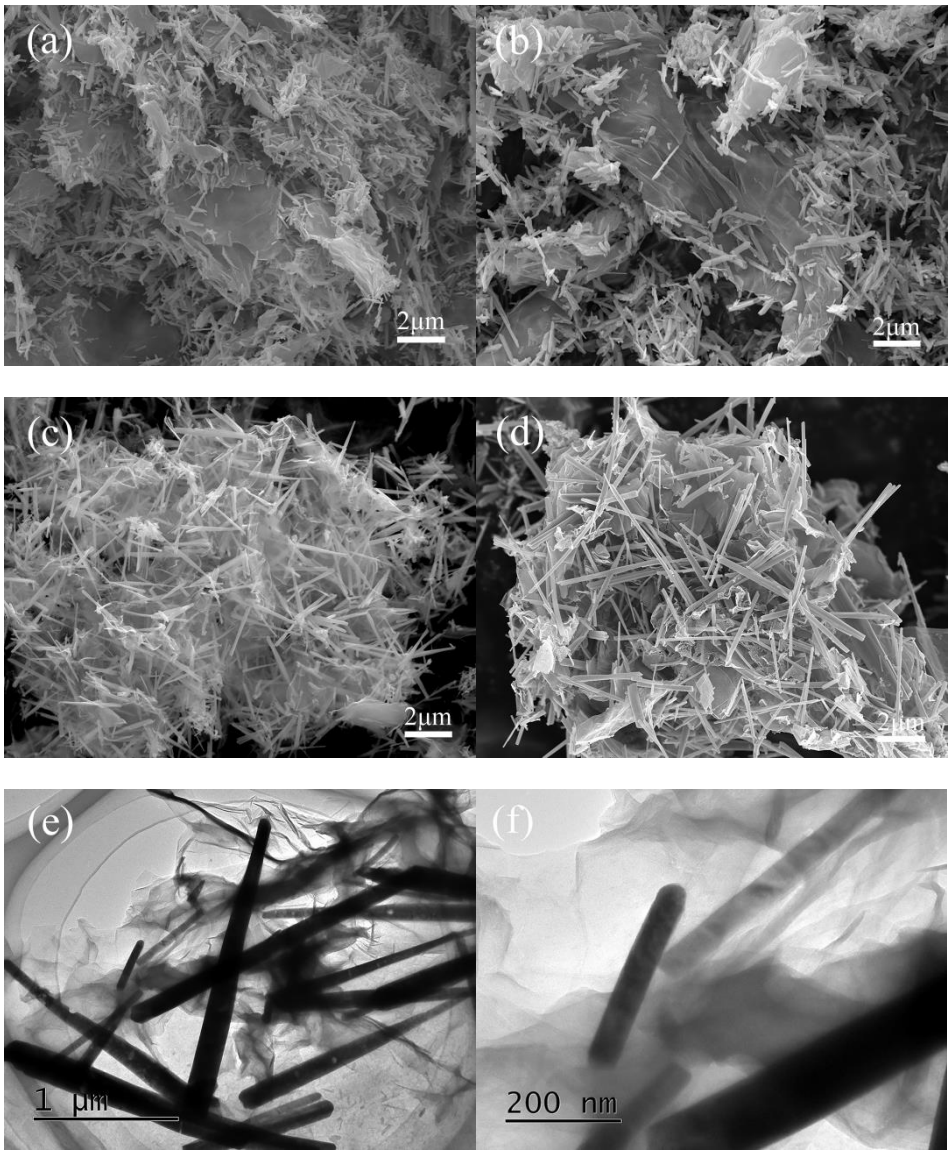

Figure 1. SEM images of Bi_2S_3/rGO-1 (**a**), Bi_2S_3/rGO-2 (**b**), Bi_2S_3/rGO-3 (**c**), Bi_2S_3/rGO-4 (**d**); TEM images of Bi_2S_3/rGO-3 (**e**,**f**).

Figure 2a shows XRD patterns of the GO, rGO, Bi_2S_3, and Bi_2S_3/rGO composite materials. After the hydrothermal treatment in the presence of thiourea, the typical diffraction peak of GO sample at 2θ = 10.2° disappeared; and the presence of the broad peak at 23.9° corresponding to the (002) plane of rGO indicates the conversion of GO to rGO [30,31]. On the other hand, the diffraction peaks of all Bi_2S_3/rGO samples match with the typical peaks of Bi_2S_3 in the CPDS card (No. 17-0320), indicating that GO used in the synthesis promotes the crystal growth of Bi_2S_3. However, the intensity of the peaks of Bi_2S_3/rGO gradually decreased with increasing amounts of GO, which is probably due to the shielding effect of rGO on the Bi_2S_3 surface [32]. Moreover, no pronounced diffraction peak of rGO has been found in XRD patterns of Bi_2S_3/rGO composites, which can be attributed to the relatively low intensity of the rGO peak or the face-to-face stacking of Bi_2S_3 on both sides [33].

Figure 2b shows the typical Raman spectra of GO, Bi_2S_3, and Bi_2S_3/rGO-3 in the range of 150–2000 cm^{-1}. The low-intensity feature at 239 cm^{-1} and the peak at 974 cm^{-1} observed for pure Bi_2S_3 correspond to the A_g optical phonon modes and surface phonon modes [34]. Similar peaks of pure Bi_2S_3 and GO can be observed in the spectra recorded on the Bi_2S_3/rGO-3 sample, indicating that rGO and Bi_2S_3 are present in Bi_2S_3/rGO. The typical G band and D band of Bi_2S_3/rGO and GO are attributed to the E_{2g} phonon of

sp^2 carbon atoms and the A_{1g} (breathing mode) of sp^3 vibrations resulting from surface defects and the structural disorder of GO, respectively [35]. The intensity ratio (I_D/I_G) of Bi_2S_3/rGO is higher than that of GO because of the increasing sp^2 domains from the reduction of GO during the hydrothermal process [36]. The Raman spectra proved the structural integrity of Bi_2S_3/rGO composites.

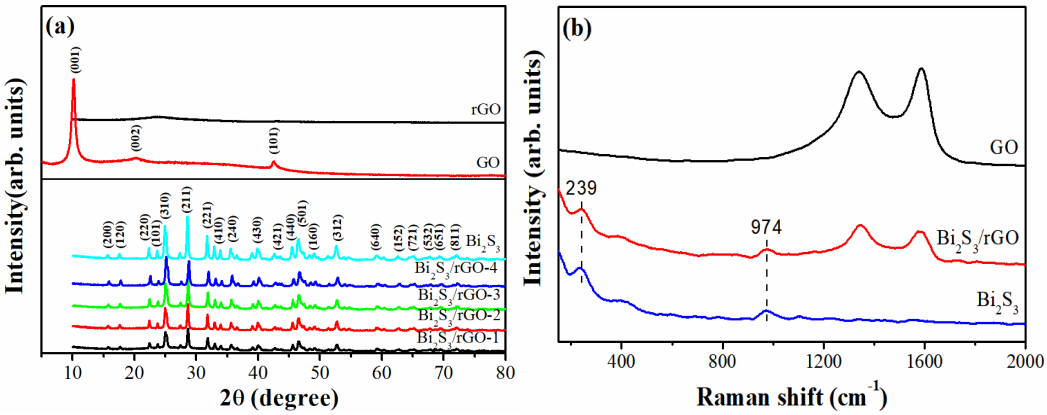

Figure 2. (**a**) The XRD spectra of the GO, rGO, Bi_2S_3, and Bi_2S_3/rGO; (**b**) Typical Raman spectra of GO, Bi_2S_3, and prepared Bi_2S_3/rGO.

The chemical composition of the samples was evaluated by X-ray photoelectron spectroscopy. Figure 3a shows the XPS survey spectra recorded on the surface of Bi_2S_3 and Bi_2S_3/rGO-3 samples. The presence of C, Bi, S, and O elements is confirmed. Compared with the pristine Bi_2S_3 sample, the intensities of C and O peaks are relatively higher in Bi_2S_3/rGO-3, suggesting the presence of rGO [37]. Figure 3b shows the XPS spectra of Bi 4f photoelectrons, in pure Bi_2S_3, the two intense peaks can be associated with Bi $4f_{7/2}$ and Bi $4f_{5/2}$ doublet with a spin-orbit splitting of 5.3 eV. The Bi 4f doublet with components at 158.2 and 163.5 eV can be observed in the Bi_2S_3/rGO-3 sample, as well as two low intensity peaks centered at 159.1 and 164.3 eV belonging to Bi-O bond, suggesting the Bi^{3+} ions interaction with rGO [38,39]. The Bi-O associated doublet peak is also observed in the pure Bi_2S_3 sample indicating that a low amount of oxygen reacted with surface Bi ions. Moreover, the S $2p_{3/2}$ and S $2p_{1/2}$ doublet peaks centered at 161.1 and 162.2 eV indicate that S^{2-} as the primary valence state occurs in Bi_2S_3/rGO-3 [40]. Figure 3c shows three components of C1s centered at 284.8, 285.9, and 288.9eV corresponding to the C=C, C–O–C, and O–C=O carbon chemical environments, respectively, indicating the residual oxygen functional groups on the surface of rGO [41]. Besides, the corresponding O 1s core-level spectrum of the Bi_2S_3/rGO-3 sample (Figure 3d) is well reproduced with three components: the peak at the lowest binding energy can be assigned to Bi-O species, and the peaks centered at 531.8 and 533.6 eV are attributed to C=O and O–C=O bonding environments, respectively [42]. Therefore, from the XPS analysis, we can suggest that Bi_2S_3 nanorods interact with reduced graphene via the formation of Bi-O bonds, although surface oxidation forming Bi-O bonds cannot be discarded.

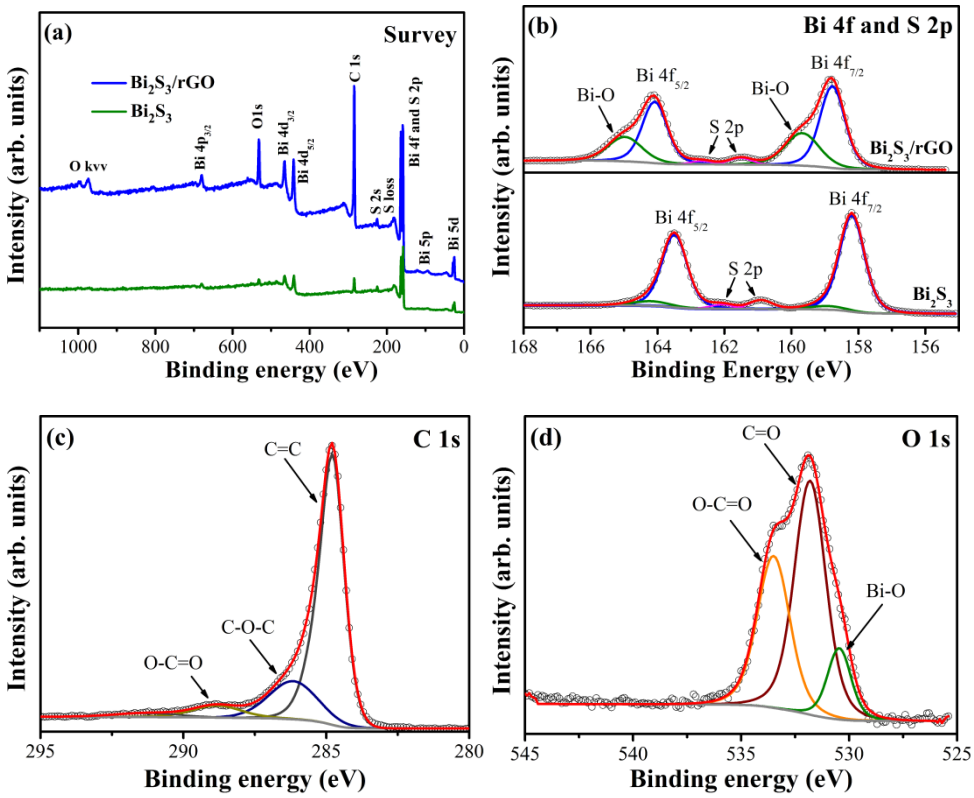

Figure 3. XPS survey spectra of (**a**) Bi_2S_3, and Bi_2S_3/rGO-3 and core-level XPS spectra of (**b**) Bi 4f and S 2p, (**c**) C1s, (**d**) O1s in Bi_2S_3/rGO-3.

FTIR spectroscopy was used to study graphene oxide and Bi_2S_3/rGO functional groups (Figure 4). The broad absorption band centered at 3425 cm^{-1} is assigned to the stretching vibration of -OH groups from adsorbed water molecules [43]. The characteristic peaks ascribed to C=O, C=C, C–O–C, and C–O functional groups were located at 1711 cm^{-1}, 1564 cm^{-1}, 1165 cm^{-1}, and 1051cm^{-1}, respectively [44,45]. Compared with GO, it is clearly seen that the intensities of the corresponding absorption peaks of Bi_2S_3/rGO sample decreased, indicating the conversion of GO to rGO during the hydrothermal process, in agreement with the Raman results.

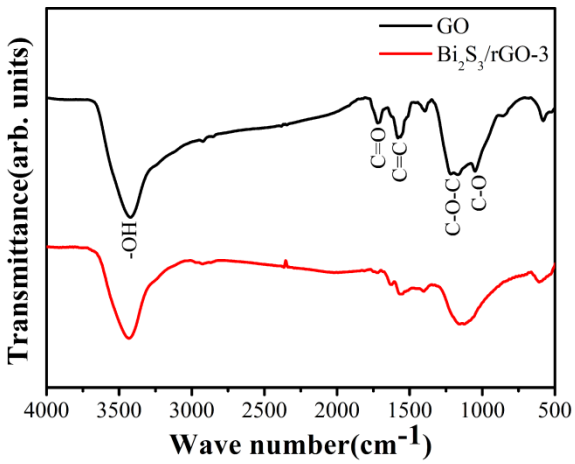

Figure 4. FTIR spectra of GO and Bi_2S_3/rGO-3 composite.

3.2. Formation Mechanism of Bi_2S_3/rGO

Based on the above analyses, the overall synthetic procedure of Bi_2S_3/rGO and the electrochemical sensing process for Ascorbic Acid (AA) can be seen in Scheme 1. First, the positively charged Bi^{3+} ions absorb the negatively charged oxygen-containing functional groups of GO sheets via electrostatic interaction [46], while the thiourea added as the sulfur source and reducing agent hydrolyzes to S^{2-} ions at high temperature. The interaction between Bi^{3+} and S^{2-} ions generates Bi_2S_3 nucleii which grow into Bi_2S_3 nanorods on the surface of the rGO to form Bi_2S_3/rGO composites [47]. The electrocatalytic response of AA at Bi_2S_3/rGO/GCE is performed in 0.1 M PBS (pH = 7.0). The oxidation process of AA with a two-electron and two-proton electro-oxidation process leads to dehydroascorbic acid formation followed by its electrochemical sensing [48].

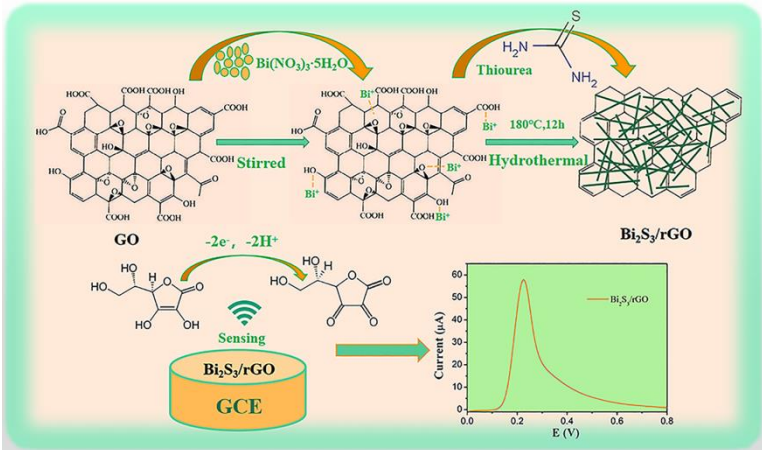

Scheme 1. Proposed growth mechanism of Bi_2S_3/rGO and the electrochemical oxidation of AA.

3.3. Bi_2S_3/rGO Electrochemical Evaluation

The electrochemical behavior of the different modified electrodes was evaluated via cyclic voltammetry (CV) and electrochemical impedance spectroscopy (EIS) using ferro/ferricyanide as the redox probe. From Figure 5a, it can be seen that compared with bare GCE, Bi_2S_3/GCE, and rGO/GCE, the Bi_2S_3/rGO/GCE shows a dramatic enhancement of the peak current, indicating that Bi_2S_3/rGO as the active layer plays a vital role for electron transfer behavior. Moreover, Bi_2S_3/rGO-3/GCE presents the optimal current response in 0.1 M KCl using 5 mM $[Fe(CN)_6]^{3-/4-}$ within the potential range of −0.2 to 0.8 V. The electrochemical impedance spectroscopy (EIS) Nyquist plots obtained for different modified electrodes are presented in Figure 5b,c. The straight line of Bi_2S_3/rGO has the steepest slope in the lower frequency area, suggesting that the synthesized Bi_2S_3/rGO composites have the minimum diffusion resistance. According to the Nyquist plots' semicircle evaluating the interfacial charge transfer resistance (Rct), the Bi_2S_3/rGO-3/GCE has a lower electron transfer resistance than that of the bare GCE and the Bi_2S_3/GCE [49,50]. This phenomenon can be associated with the introduction of Bi_2S_3 nanorods improving electron transfer capability. Compared to the Bi_2S_3/rGO-1/GCE, the Bi_2S_3/rGO-2/GCE and the Bi_2S_3/rGO-4/GCE, Bi_2S_3/rGO-3/GCE have better conductivity (Figure 5c). According to the obtained results, the interfacial charge transfer resistance of the Bi_2S_3/rGO composites decreases in sequence along with the increase in the amount of GO added to the synthesis. This can be attributed to the graphene that facilitates the transport of electrons and ions. However, adding high amounts of GO increased the composite resistance, which is likely related to the morphology of the Bi_2S_3 nanorods. The longer length of the nanorods increases the distance between rGO nanosheets retarding facile electron transport [45]. Hence, the Bi_2S_3/rGO-3 was chosen in the following experiments.

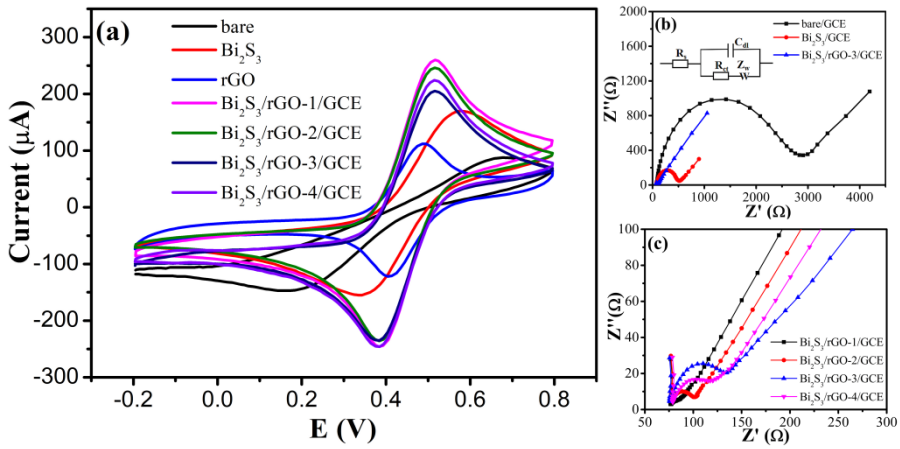

Figure 5. (**a**) CVs of bare GCE, Bi_2S_3/GCE, GO/GCE, Bi_2S_3/rGO-1/GCE, Bi_2S_3/rGO-2/GCE, Bi_2S_3/rGO-3/GCE, and Bi_2S_3/rGO-4/GCE in 0.1 M KCl containing 5 mM $[Fe(CN)_6]^{3-/4-}$; (**b**) EIS of bare GCE, Bi_2S_3/GCE, and Bi_2S_3/rGO-1/GCE; (**c**) EIS of Bi_2S_3/rGO-1/GCE, Bi_2S_3/rGO-2/GCE, Bi_2S_3/rGO-3/GCE, and Bi_2S_3/rGO-4/GCE. The inset in (**b**) represents the equivalent circuit model.

In order to investigate the electrocatalytic response of the different modified electrodes in the detection of AA, differential pulse voltammetry (DPV) was carried out in 0.1 M PBS (pH = 7.0) containing 5 mM AA at a scan rate of 100 mV s^{-1} (Figure 6). The rate of electro-oxidation on the AA was varied at different modified electrodes, the peak potential of the AA oxidation was 0.492, 0.556, 0.188, and 0.224 V for the bare GCE, Bi_2S_3/GCE, rGO/GCE, and Bi_2S_3/rGO-3/GCE, respectively. The Bi_2S_3/GCE showed a weak oxidation peak due to the electric blocking effect produced by the semiconductor's presence over the electrode surface. The Bi_2S_3/rGO-3/GCE showed an exceptional current response at 0.225 V, and the superior electrochemical performance of Bi_2S_3/rGO-3/GCE can be attributed to the synergetic combination of the nanocrystalline Bi_2S_3 with the GO [51]. Therefore, it is suggested that Bi_2S_3 and rGO improve the materials' electrical conductivity and catalytic activity synergistically.

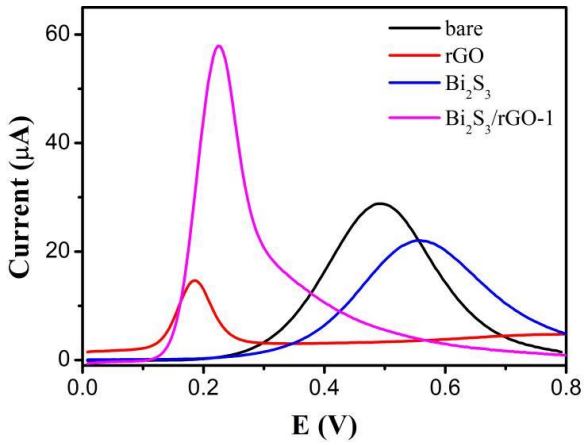

Figure 6. DPVs for bare GCE, Bi_2S_3/GCE, rGO/GCE, and Bi_2S_3/rGO-3/GCE in 0.1 M PBS (pH = 7.0) with AA concentrations 5 mM.

3.4. Optimization of Detection Conditions

3.4.1. Effect of Solution pH

To evaluate the pH effect on the response to the electrochemical behavior of AA on the Bi_2S_3/rGO-3/GCE, analyses were carried out in the pH range from 3.0 to 8.0. As shown in Figure 7a, the oxidation peak potential (E_P) shifts towards greater negative potential for increasing pH values, indicating that the electro-oxidation process is pH-dependent

and protons take part in the electrode reaction [52,53]. The oxidation peak current of AA increases steadily as the pH changes from 3.0 to 4.0 (Figure 7b); however, further increasing the pH value from 4.0 to 8.0, the anode peak current tends to decrease. The high analytical signal for AA is observed at pH 4.0. The dependence of the AA peak potential on pH can be expressed by Equation (1):

$$E_P\ (\mathrm{V}) = -0.0484\ \mathrm{pH} + 0.714,\ (\mathrm{R}^2 = 0.998) \quad (1)$$

In Figure 7c, the slope is a Nernstian value of −0.0484 V/pH, which indicates the participation of electron and proton involving in the process of AA on the Bi_2S_3/rGO-3/GCE surface [54].

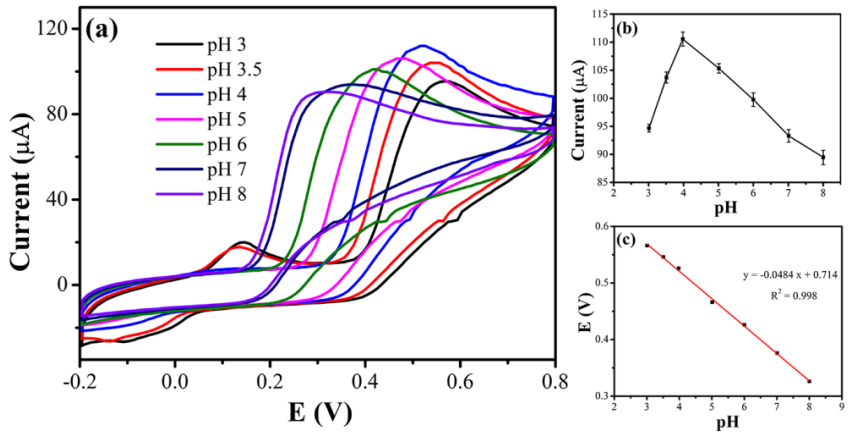

Figure 7. (**a**) CVs of Bi_2S_3/rGO-3/GCE in the presence of 5 mM AA comprising of various pH solutions from 3 to 8 at a scan rate of 100 mV s^{-1}; (**b**) The plot of I_P vs. pH value, and (**c**) E_P vs. pH value.

3.4.2. Effect of Scan Rate

The AA oxidation reaction kinetics of Bi_2S_3/rGO-3/GCE was studied by CVs at a scan rate range of 20–100 mV s^{-1}. As shown in Figure 8a, the peak current response increases with the increase in scan rate and the peak potential shifts to the positive side. Furthermore, the linear relationship between the oxidation peak current (I_P) and the square roots of scan rates can be seen in Figure 8b, and the linear regression equation was described as follows:

$$I_P\ (\mathrm{A}) = 9.85\ v^{1/2} + 25.64\ (v \text{ in mV s}^{-1}),\ \mathrm{R}^2 = 0.994 \quad (2)$$

The oxidation peak currents are well proportional to the square roots of the scan rates, which indicates that the oxidation reaction of AA is a typical diffusion-controlled process [55].

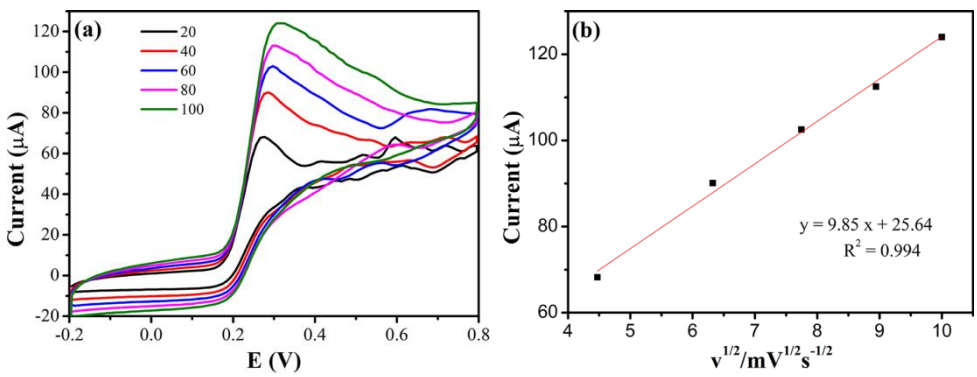

Figure 8. (**a**) CV response of 5 MM of AA for different scan rates ranging from 20 to 100 mV s^{-1} at Bi_2S_3/rGO-3/GCE in 0.1 M PBS solution (pH = 7.0), (**b**) The plots of the peak current vs. square roots of scan rates ($v^{1/2}$).

3.5. Analytical Sensing Performance

Differential pulse voltammograms (DPVs) of the Bi_2S_3/rGO-3/GCE for AA in the PBS solution was studied, and the obtained DPV profiles are presented in Figure 9a. The peak current increases linearly with the concentration ranging from 5 μM to 1200 μM (Figure 9b) and can be described by the corresponding Equation (3):

$$I_p\ (\mu A) = 0.01898\ C\ (\mu M) - 0.2550\ (\mu A)\ (R = 0.996) \quad (3)$$

From this data, the detection limit of the Bi_2S_3/rGO-3/GCE is 2.94 μM (S/N = 3) for the electrochemical detection of AA, and a sensitivity of 268.84 μA mM^{-1} cm^{-2} was determined. Comparison of the analytical results of the Bi_2S_3/rGO-3/GCE and reported results for ascorbic acid sensors are summarized in Table 1. From this table, the electrocatalytic activity of the Bi_2S_3/rGO-3/GCE sensor is comparable or better than for recently reported studies using other materials.

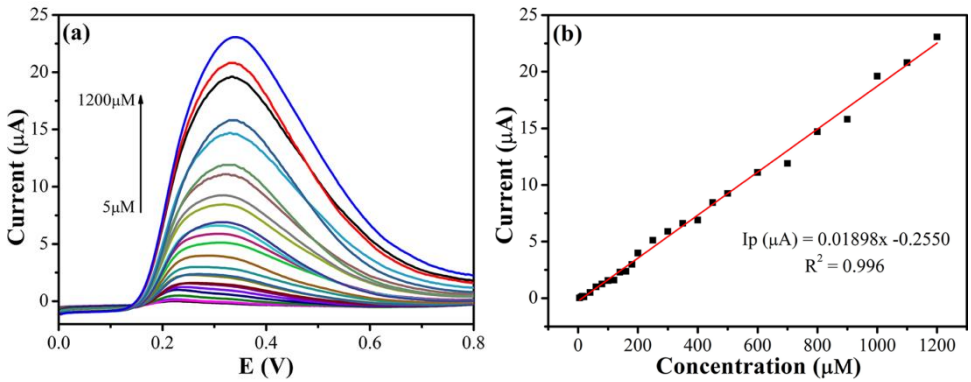

Figure 9. (**a**) DPV responses of Bi_2S_3/rGO-3/GCE in the presence of AA in concentrations ranging from 5 μM to 1200 μM; (**b**)The plot of anodic peak current versus different concentration values.

Table 1. The performance in AA detection using Bi_2S_3/rGO-3/GCE, in comparison with other reported materials.

Modified Materials	LOD (μM)	Linear Range (μM)	Reference (μA mM^{-1} cm^{-2})	Reference
Bi_2S_3/TNF	-	1000–10,000	38	[51]
GO/$TmPO_4$	39	100–1000	—	[56]
NP-Cu/RGO/GCE	0.09	0.5–30	—	[57]
MoS2-PANI/rGO	22.2	50–8000	48.2	[58]
rGO/GCE	4.7	65–2530	—	[59]
Pd NWs/GCE	0.2	25–900	166.5	[60]
PCN/ GO	3.7	30–3000	380	[61]
Bi_2S_3/rGO	2.94	5–1200	268.84	This work

3.6. Reproducibility and Stability

The reproducibility and stability of the Bi_2S_3/rGO-3/GCE were examined in 0.1 M PBS (pH = 7), adding a fixed amount of AA (1 mM) (Figure 10). In five independently prepared electrode tests, the relative standard deviation (RSD) obtained of the peak current was 6.25%, which is within acceptable levels. Moreover, the current response of Bi_2S_3/rGO-3/GCE was 96.4% of its initial current value after twenty DPV tests, which implies adequate operational stability.

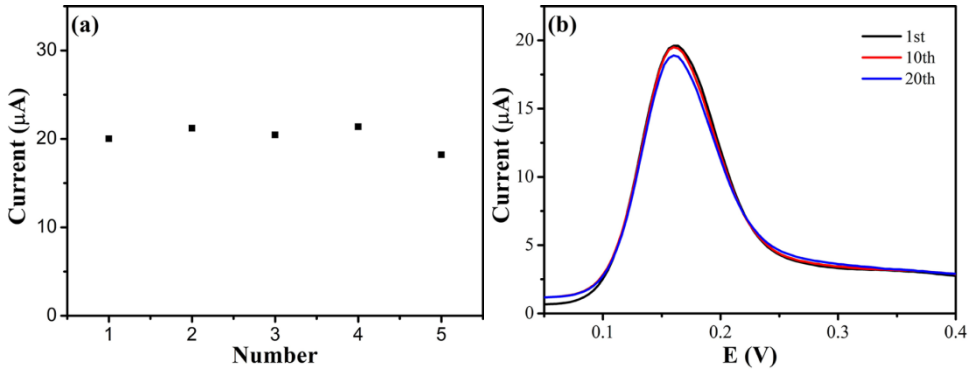

Figure 10. DPVs of Bi_2S_3/rGO-3/GCE in 0.1 M PBS containing 1 mM AA (**a**) for five independently prepared electrodes, and (**b**) the current responses of the 1st, 10th, and 20th cycle.

3.7. Interference Effect

The selectivity of the target analyte is a significant property for a biosensor. The interference experiments were carried out by successive addition of 200 μM AA and 200 μM interfering species (glucose, carbamide, clycine, K^+, Na^+, Mg^{2+}, Zn^{2+}, dopamine (DA), and uric acid (UA)) in 0.1 mM PBS (pH = 7.0). The measured effects of different interferents along with AA are shown in Figure 11. As shown in this figure, all these organic and inorganic species did not show any significant fluctuation in the determination of AA. The current response was obviously enhanced when 200 μM AA was added again. These results indicate that Bi_2S_3/rGO-3/GCE has high sensitivity and selectivity to AA in the presence of other organic molecules and ions normally found in food and biological samples.

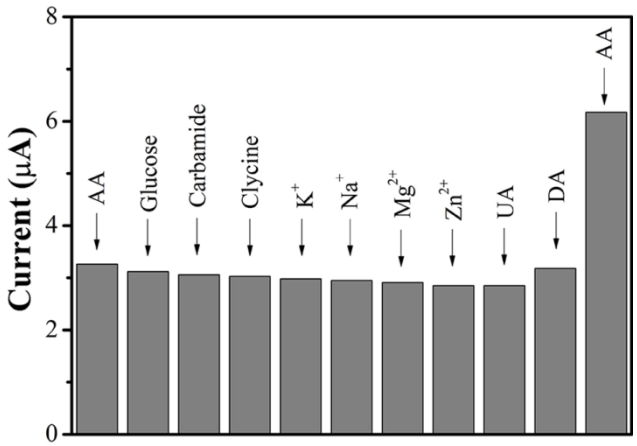

Figure 11. The amperometric response of the Bi_2S_3/rGO-3/GCE electrode towards the addition of 200 μM AA and various interfering compounds in 0.1 M PBS.

3.8. AA Analytical Application

The applicability of Bi_2S_3/rGO-3/GCE was further examined using vitamin C tablets. Experiments were performed with the standard addition method [62] and recoveries in the range of 97.14–101.55% were obtained (Table 2). The good recovery values for AA indicate the feasible application of the Bi_2S_3/rGO-3/GCE electrode for the AA determination in real samples.

Table 2. Determination of AA in vitamin C tablets (n = 3).

Sample	Added (μM)	Found (μM)	Recovery (%)	RSD (%)
Vitamin C tablets	0	<LOD	-	-
	200	203.11	101.55	2.25
	300	297.42	98.26	1.58
	400	388.57	97.14	3.04
	500	487.62	97.42	2.71

RSD (%) = (Standard deviation/The average of the data obtained by repeating 3 times) × 100%.

4. Conclusions

In summary, using a one-pot synthesis method Bi_2S_3/rGO composites were successfully synthesized. The obtained Bi_2S_3/rGO composites were used as the sensor active layer significantly improving the GCE performance in detecting AA. The size of the Bi_2S_3 rods can be controlled by adjusting the amount of GO in the synthesis, and the synergistic effect between rGO sheets and Bi_2S_3 nanorods has an essential effect on the electrochemical performance. The suitably sized nanorods of Bi_2S_3 anchored on rGO as an electrochemical sensor to detect AA show excellent sensitivity, good selectivity and stability, as well as good reproducibility and a detection limit of 2.94 μM. Moreover, using Bi_2S_3/rGO/GCE as a sensor to detect an actual sample containing AA, a good recovery (97.1% to 101.55%) was observed. The research method described in this work opens new avenues for optimizing novel materials to be used as the active layer in electrochemical detection.

Supplementary Materials: The following are available online at https://www.mdpi.com/article/10.3390/chemosensors9080190/s1, Figure S1: Cyclic voltammetry curves of Bi_2S_3 modified glassy carbon electrodes prepared using different sulfur sources, Figure S2: SEM images of Bi_2S_3 prepared using different sulfur sources, Figure S3: Bi_2S_3/rGO-3 Element mapping image and the EDAX spectrum.

Author Contributions: Investigation, data curation, writing—original draft, C.Q.; methodology, H.L. and S.Z.; validation, supervision, C.W. and R.S.; visualization, writing—review and editing, C.B. and G.L.; conceptualization, supervision, writing—review and editing, W.L. All authors have read and agreed to the published version of the manuscript.

Funding: This research was partially funded by the National Natural Science Foundation of China (Nos. U1764254 and 21911530255), 111 Project, China (No. D17003), and the Open Research Fund of the State Key Laboratory of Inorganic Synthesis and Preparative Chemistry (Jilin University, Grant No. 2021-03). C.B. thanks the Belgian Fund for Scientific Research under the FRFC contract CDR J001019. C.B. is a research associate of the National Funds for Scientific Research (FRS-FNRS, Belgium).

Institutional Review Board Statement: Not applicable.

Informed Consent Statement: Not applicable.

Data Availability Statement: Not applicable.

Conflicts of Interest: The authors declare no conflict of interest.

References

1. Meng, H.J.; Yang, D.Q.; Tu, Y.F.; Yan, J.L. Turn-on fluorescence detection of ascorbic acid with gold nanolcusters. *Talanta* **2017**, *165*, 346–350. [CrossRef] [PubMed]
2. Peng, J.; Ling, J.; Zhang, X.Q.; Zhang, L.Y.; Cao, Q.E.; Ding, Z.T. A rapid, sensitive and selective colorimetric method for detection of ascorbic acid. *Sens. Actuat B Chem.* **2015**, *221*, 708–716. [CrossRef]
3. Granero, A.M.; Pierini, G.D.; Robledo, S.N.; Di Nezio, M.S.; Fernandez, H.; Zon, M.A. Simultaneous determination of ascorbic and uric acids and dopamine in human serum samples using three-way calibration with data from square wave voltammetry. *Microchem. J.* **2016**, *129*, 205–212. [CrossRef]
4. Uzun, D.; Gunduzalp, A.B.; Hasdemir, E. Selective determination of dopamine in the presence of uric acid and ascorbic acid by N, N′-bis(indole-3-carboxaldimine)-1,2-diaminocyclohexane thin film modified glassy carbon electrode by differential pulse voltammetry. *J. Electroanal Chem.* **2015**, *747*, 68–76. [CrossRef]

5. Nellaiappan, S.; Kumar, A.S. Reductive cleavage of methyl orange under formation of a redox-active hydroquinone/polyaniline nanocomposite on an electrode modified with MWCNTs, and its application to flow injection analysis of ascorbic acid at low potential and neutral pH value. *Microchim. Acta* **2017**, *184*, 3255–3264. [CrossRef]
6. Sena, M.M.; Fernandes, J.C.B.; Rover, L.; Poppi, R.J.; Kubota, L.T. Application of two- and three-way chemometric methods in the study of acetylsalicylic acid and ascorbic acid mixtures using ultraviolet spectrophotometry. *Anal. Chim. Acta* **2000**, *409*, 159–170. [CrossRef]
7. Hossu, A.M.; Cristiana, R.; Ioniţă, I.; Magearu, V. Determination of the vitamin D in pharmaceuticals by high performance liquid chromatography. *Rev. Chim. Buchar. Orig. Ed.* **2004**, *55*, 788–790.
8. Zhang, H.; Huang, F.; Xu, S.; Xia, Y.; Huang, W.; Li, Z. Fabrication of nanoflower-like dendritic Au and polyaniline composite nanosheets at gas/liquid interface for electrocatalytic oxidation and sensing of ascorbic acid. *Electrochem. Commun.* **2013**, *30*, 46–50. [CrossRef]
9. Liu, Q.; Zhu, X.; Huo, Z.H.; He, X.L.; Liang, Y.; Xu, M.T. Electrochemical detection of dopamine in the presence of ascorbic acid using PVP/graphene modified electrodes. *Talanta* **2012**, *97*, 557–562. [CrossRef]
10. Li, L.; Zhang, P.; Li, Z.; Li, D.; Han, B.; Tu, L.; Li, B.; Wang, Y.; Ren, L.; Yang, P.; et al. CuS/Prussian blue core-shell nanohybrid as an electrochemical sensor for ascorbic acid detection. *Nanotechnology* **2019**, *30*, 325501. [CrossRef]
11. Li, F.; Tang, C.; Liu, S.; Ma, G. Development of an electrochemical ascorbic acid sensor based on the incorporation of a ferricyanide mediator with a polyelectrolyte–calcium carbonate microsphere. *Electrochim. Acta* **2010**, *55*, 838–843. [CrossRef]
12. Sivanesan, A.; Kannan, P.; Abraham John, S. Electrocatalytic oxidation of ascorbic acid using a single layer of gold nanoparticles immobilized on 1,6-hexanedithiol modified gold electrode. *Electrochim. Acta* **2007**, *52*, 8118–8124. [CrossRef]
13. Qian, L.; Gao, Q.; Song, Y.; Li, Z.; Yang, X. Layer-by-layer assembled multilayer films of redox polymers for electrocatalytic oxidation of ascorbic acid. *Sens. Actuators B Chem.* **2005**, *107*, 303–310. [CrossRef]
14. Kul, D.; Ghica, M.E.; Pauliukaite, R.; Brett, C.M. A novel amperometric sensor for ascorbic acid based on poly (Nile blue A) and functionalised multi-walled carbon nanotube modified electrodes. *Talanta* **2013**, *111*, 76–84. [CrossRef] [PubMed]
15. Li, F.; Li, J.; Feng, Y.; Yang, L.; Du, Z. Electrochemical behavior of graphene doped carbon paste electrode and its application for sensitive determination of ascorbic acid. *Sens. Actuators B Chem.* **2011**, *157*, 110–114. [CrossRef]
16. Gao, J.; He, P.; Yang, T.T.; Zhou, L.H.; Wang, X.J.; Chen, S.X.; Lei, H.; Zhang, H.; Jia, B.; Liu, J.F. Electrodeposited NiO/graphene oxide nanocomposite: An enhanced voltammetric sensing platform for highly sensitive detection of uric acid, dopamine and ascorbic acid. *J. Electroanal Chem.* **2019**, 852. [CrossRef]
17. Konstantatos, G.; Levina, L.; Tang, J.; Sargent, E.H. Sensitive Solution-Processed Bi_2S_3 Nanocrystalline Photodetectors. *Nano Lett.* **2008**, *8*, 4002–4006. [CrossRef]
18. Kumar, B.G.; Srinivas, B.; Muralidharan, K. Photo-responsive Bi_2S_3 nanoflakes: Synthesis and device fabrication at ambient conditions. *Mater. Res. Bull.* **2017**, *89*, 108–115. [CrossRef]
19. Yang, X.Y.; Tian, S.S.; Li, R.; Wang, W.; Zhou, S.M. Use of single-crystalline Bi_2S_3 nanowires as room temperature ethanol sensor synthesized by hydrothermal approach. *Sens. Actuat B-Chem.* **2017**, *241*, 210–216. [CrossRef]
20. Dutta, A.K.; Maji, S.K.; Mitra, K.; Sarkar, A.; Saha, N.; Ghosh, A.B.; Adhikary, B. Single source precursor approach to the synthesis of Bi_2S_3 nanoparticles: A new amperometric hydrogen peroxide biosensor. *Sens. Actuators B Chem.* **2014**, *192*, 578–585. [CrossRef]
21. Bernechea, M.; Miller, N.C.; Xercavins, G.; So, D.; Stavrinadis, A.; Konstantatos, G. Solution-processed solar cells based on environmentally friendly $AgBiS_2$ nanocrystals. *Nat. Photonics* **2016**, *10*, 521. [CrossRef]
22. Gao, F.; Song, J.; Zhang, B.; Tanaka, H.; Gao, F.; Qiu, W.W.; Wang, Q.X. Synthesis of core-shell structured Au@Bi_2S_3 nanorod and its application as DNA immobilization matrix for electrochemical biosensor construction. *Chin. Chem. Lett.* **2020**, *31*, 181–184. [CrossRef]
23. Stankovich, S.; Dikin, D.A.; Dommett, G.H.B.; Kohlhaas, K.M.; Zimney, E.J.; Stach, E.A.; Piner, R.D.; Nguyen, S.T.; Ruoff, R.S. Graphene-based composite materials. *Nature* **2006**, *442*, 282–286. [CrossRef]
24. Chen, D.; Feng, H.B.; Li, J.H. Graphene Oxide: Preparation, Functionalization, and Electrochemical Applications. *Chem. Rev.* **2012**, *112*, 6027–6053. [CrossRef]
25. Luo, J.; Jiang, S.; Zhang, H.; Jiang, J.; Liu, X. A novel non-enzymatic glucose sensor based on Cu nanoparticle modified graphene sheets electrode. *Anal. Chim. Acta* **2012**, *709*, 47–53. [CrossRef] [PubMed]
26. Guo, X.R.; Yue, H.Y.; Song, S.S.; Huang, S.; Gao, X.; Chen, H.T.; Wu, P.F.; Zhang, T.; Wang, Z.Z. Simultaneous electrochemical determination of dopamine and uric acid based on MoS_2 nanoflowers-graphene/ITO electrode. *Microchem. J.* **2020**, 154.
27. Yan, X.; Gu, Y.; Li, C.; Zheng, B.; Li, Y.; Zhang, T.; Zhang, Z.; Yang, M. Morphology-controlled synthesis of Bi_2S_3 nanorods-reduced graphene oxide composites with high-performance for electrochemical detection of dopamine. *Sens. Actuators B Chem.* **2018**, *257*, 936–943. [CrossRef]
28. Hummers, W.S.; Offeman, R.E. Preparation of Graphitic Oxide. *J. Am. Chem. Soc.* **1958**, *80*, 1339. [CrossRef]
29. Park, S.K.; Woo, S.; Lee, S.; Seong, C.Y.; Piao, Y. Design and tailoring of three-dimensional graphene-Vulcan carbon-Bi_2S_3 ternary nanostructures for high-performance lithium-ion-battery anodes. *Rsc. Adv.* **2015**, *5*, 52687–52694. [CrossRef]
30. Lambert, T.N.; Luhrs, C.C.; Chavez, C.A.; Wakeland, S.; Brumbach, M.T.; Alam, T.M. Graphite oxide as a precursor for the synthesis of disordered graphenes using the aerosol-through-plasma method. *Carbon* **2010**, *48*, 4081–4089. [CrossRef]
31. Li, C.; Zhao, J.Y.; Yan, X.Y.; Gu, Y.; Liu, W.L.; Tang, L.; Zheng, B.; Li, Y.R.; Chen, R.X.; Zhang, Z.Q. Tremella-like graphene-Au composites used for amperometric determination of dopamine. *Analyst* **2015**, *140*, 1913–1920. [CrossRef]

32. Wang, Y.; Li, Z.; Tian, Y.F.; Zhao, W.; Liu, X.Q.; Yang, J.B. A facile way to fabricate graphene sheets on TiO2 nanotube arrays for dye-sensitized solar cell applications. *J. Mater. Sci.* **2014**, *49*, 7991–7999. [CrossRef]
33. Heshmatynezhad, L.; Jamali-Sheini, F.; Monshi, A. UV-assisted sonochemical synthesis and optoelectrical properties of Bi_2S_3/rGO nanocomposites. *Ceram. Int.* **2019**, *45*, 13923–13933. [CrossRef]
34. Deshpande, M.P.; Sakariya, P.N.; Bhatt, S.V.; Garg, N.; Patel, K.; Chaki, S.H. Characterization of Bi_2S_3 nanorods prepared at room temperature. *Mat. Sci. Semicon Proc.* **2014**, *21*, 180–185. [CrossRef]
35. Ferrari, A.C.; Robertson, J. Interpretation of Raman spectra of disordered and amorphous carbon. *Phys. Rev. B* **2000**, *61*, 14095–14107. [CrossRef]
36. How, G.T.S.; Pandikumar, A.; Ming, H.N.; Ngee, L.H. Highly exposed {001} facets of titanium dioxide modified with reduced graphene oxide for dopamine sensing. *Sci Rep.* **2014**, *4*, 1–8. [CrossRef]
37. Gote, G.H.; Bhopale, S.R.; More, M.A.; Late, D.J. Realization of Efficient Field Emitter Based on Reduced Graphene Oxide-Bi_2S_3 Heterostructures. *Phys. Status Solidi A* **2019**, *216*, 1900121. [CrossRef]
38. Luo, W.; Li, F.; Li, Q.D.; Wang, X.P.; Yang, W.; Zhou, L.; Mai, L.Q. Heterostructured Bi_2S_3-Bi_2O_3 Nanosheets with a Built-In Electric Field for Improved Sodium Storage. *Acs Appl. Mater. Inter.* **2018**, *10*, 7201–7207. [CrossRef]
39. Kubendhiran, S.; Karikalan, N.; Chen, S.-M.; Sundaresan, P.; Karthik, R. Synergistic activity of single crystalline bismuth sulfide and sulfur doped graphene towards the electrocatalysis of tryptophan. *J. Catal.* **2018**, *367*, 252–263. [CrossRef]
40. Wang, X.T.; Lv, R.; Wang, K. Synthesis of ZnO@ZnS-Bi_2S_3 core-shell nanorod grown on reduced graphene oxide sheets and its enhanced photocatalytic performance. *J. Mater. Chem A* **2014**, *2*, 8304–8313.
41. Lim, S.P.; Pandikumar, A.; Lim, Y.S.; Huang, N.M.; Lim, H.N. In-situ electrochemically deposited polypyrrole nanoparticles incorporated reduced graphene oxide as an efficient counter electrode for platinum-free dye-sensitized solar cells. *Sci Rep.* **2014**, *4*, 1–7. [CrossRef] [PubMed]
42. Nie, G.D.; Lu, X.F.; Lei, J.Y.; Yang, L.; Wang, C. Facile and controlled synthesis of bismuth sulfide nanorods-reduced graphene oxide composites with enhanced supercapacitor performance. *Electrochim. Acta* **2015**, *154*, 24–30. [CrossRef]
43. He, H.Y. Facile synthesis of Bi_2S_3 nanocrystalline-modified TiO_2: Fe nanotubes hybrids and their photocatalytic activities in dye degradation. *Part. Sci. Technol.* **2017**, *35*, 410–417. [CrossRef]
44. Guo, H.L.; Wang, X.F.; Qian, Q.Y.; Wang, F.B.; Xia, X.H. A Green Approach to the Synthesis of Graphene Nanosheets. *Acs. Nano* **2009**, *3*, 2653–2659. [CrossRef] [PubMed]
45. Feng, B.; Xie, J.; Cao, G.S.; Zhu, T.J.; Zhao, X.B. Facile synthesis of ultrafine $CoSn_2$ nanocrystals anchored on graphene by one-pot route and the improved electrochemical Li-storage properties. *New J. Chem.* **2013**, *37*, 474–480. [CrossRef]
46. Zhang, K.; Wang, Y.Y.; Liu, P.; Li, W. Chemical fabrication and electrochemical performance of Bi2S3-nanorods charged reduced graphene oxide. *Mater. Lett.* **2015**, *161*, 774–777. [CrossRef]
47. Chen, Y.J.; Tian, G.H.; Mao, G.J.; Li, R.; Xiao, Y.T.; Han, T.R. Facile synthesis of well-dispersed Bi_2S_3 nanoparticles on reduced graphene oxide and enhanced photocatalytic activity. *Appl. Surf. Sci.* **2016**, *378*, 231–238. [CrossRef]
48. Puangjan, A.; Chaiyasith, S.; Wichitpanya, S.; Daengduang, S.; Puttota, S. Electrochemical sensor based on PANI/MnO_2-Sb_2O_3 nanocomposite for selective simultaneous voltammetric determination of ascorbic acid and acetylsalicylic acid. *J. Electroanal Chem.* **2016**, *782*, 192–201. [CrossRef]
49. Tian, H.L.; Fan, H.Q.; Ma, J.W.; Liu, Z.Y.; Ma, L.T.; Lei, S.H.; Fang, J.W.; Long, C.B. Pt-decorated zinc oxide nanorod arrays with graphitic carbon nitride nanosheets for highly efficient dual-functional gas sensing. *J. Hazard. Mater.* **2018**, *341*, 102–111. [CrossRef]
50. Ray, C.; Dutta, S.; Roy, A.; Sahoo, R.; Pal, T. Redox mediated synthesis of hierarchical Bi_2O_3/MnO_2 nanoflowers: A non-enzymatic hydrogen peroxide electrochemical sensor. *Dalton T* **2016**, *45*, 4780–4790. [CrossRef]
51. Cabrita, J.F.; Ferreira, V.C.; Monteiro, O.C. Titanate nanofibers sensitized with nanocrystalline Bi_2S_3 as new electrocatalytic materials for ascorbic acid sensor applications. *Electrochim. Acta* **2014**, *135*, 121–127. [CrossRef]
52. Hashemi, S.A.; Mousavi, S.M.; Bahrani, S.; Ramakrishna, S.; Babapoor, A.; Chiang, W.H. Coupled graphene oxide with hybrid metallic nanoparticles as potential electrochemical biosensors for precise detection of ascorbic acid within blood. *Anal. Chim. Acta* **2020**, *1107*, 183–192. [CrossRef]
53. Wang, C.; Yuan, R.; Chai, Y.Q.; Chen, S.H.; Zhang, Y.; Hu, F.X.; Zhang, M.H. Non-covalent iron (III)-porphyrin functionalized multi-walled carbon nanotubes for the simultaneous determination of ascorbic acid, dopamine, uric acid and nitrite. *Electrochim. Acta* **2012**, *62*, 109–115. [CrossRef]
54. Saleh Mohammadnia, M.; Marzi Khosrowshahi, E.; Naghian, E.; Homayoun Keihan, A.; Sohouli, E.; Plonska-Brzezinska, M.E.; Ali Sobhani, N.; Rahimi-Nasrabadi, M.; Ahmadi, F. Application of carbon nanoonion-$NiMoO_4$-$MnWO_4$ nanocomposite for modification of glassy carbon electrode: Electrochemical determination of ascorbic acid. *Microchem. J.* **2020**, *159*, 105470. [CrossRef]
55. Hsu, S.C.; Cheng, H.T.; Wu, P.X.; Weng, C.J.; Santiago, K.S.; Yeh, J.M. Electrochemical Sensor Constructed Using a Carbon Paste Electrode Modified with Mesoporous Silica Encapsulating PANI Chains Decorated with GNPs for Detection of Ascorbic Acid. *Electrochim. Acta* **2017**, *238*, 246–256. [CrossRef]
56. Huang, H.P.; Yue, Y.F.; Chen, Z.Z.; Chen, Y.N.; Wu, S.Z.; Liao, J.S.; Liu, S.J.; Wen, H.R. Electrochemical sensor based on a nanocomposite prepared from $TmPO_4$ and graphene oxide for simultaneous voltammetric detection of ascorbic acid, dopamine and uric acid. *Microchim. Acta* **2019**, *186*, 1–9. [CrossRef] [PubMed]

57. Fu, J.; Zhang, Z.; Li, G. Progress on the development of DNA-mediated metal nanomaterials for environmental and biological analysis. *Chin. Chem. Lett.* **2019**, *30*, 285–291. [CrossRef]
58. Li, S.; Ma, Y.; Liu, Y.; Xin, G.; Wang, M.; Zhang, Z.; Liu, Z. Electrochemical sensor based on a three dimensional nanostructured MoS_2 nanosphere-PANI/reduced graphene oxide composite for simultaneous detection of ascorbic acid, dopamine, and uric acid. *Rsc. Adv.* **2019**, *9*, 2997–3003. [CrossRef]
59. de Faria, L.V.; Lisboa, T.P.; de Farias, D.M.; Araujo, F.M.; Machado, M.M.; de Sousa, R.A.; Matos, M.A.C.; Munoz, R.A.A.; Matos, R.C. Direct analysis of ascorbic acid in food beverage samples by flow injection analysis using reduced graphene oxide sensor. *Food Chem.* **2020**, *319*, 126509. [CrossRef]
60. Liu, H.; Guo, K.; Lv, J.; Gao, Y.; Duan, C.; Deng, L.; Zhu, Z. A novel nitrite biosensor based on the direct electrochemistry of horseradish peroxidase immobilized on porous Co_3O_4 nanosheets and reduced graphene oxide composite modified electrode. *Sens. Actuators B Chem.* **2017**, *238*, 249–256. [CrossRef]
61. Zhang, L.H.; Liu, C.D.; Wang, Q.W.; Wang, X.H.; Wang, S.T. Electrochemical sensor based on an electrode modified with porous graphitic carbon nitride nanosheets (C_3N_4) embedded in graphene oxide for simultaneous determination of ascorbic acid, dopamine and uric acid. *Microchim. Acta* **2020**, *187*, 1–10. [CrossRef] [PubMed]
62. Yari, A.; Shams, A. Silver-filled MWCNT nanocomposite as a sensing element for voltammetric determination of sulfamethoxazole. *Anal. Chim. Acta* **2018**, *1039*, 51–58. [CrossRef] [PubMed]